

# Corrosion Evaluation of the Welded Zone between Carbon Steel and Stainless Steel Embedded in Concrete and Exposed to a Marine-Like Environment

Rosalba Hernández-Leos,<sup>1</sup> J. T. Pérez-Quiroz,<sup>2</sup> M. Martínez,<sup>2</sup> J. Torres,<sup>1</sup> F. Castañeda,<sup>1</sup> J. Morales,<sup>1</sup> René Antaño<sup>1,\*</sup>

<sup>1</sup>Centro de Investigación y Desarrollo Tecnológico en electroquímica SC, Parque Tecnológico Querétaro-Sanfandila S/N, Querétaro, México, C. P. 76703.

<sup>2</sup>Instituto Mexicano del Transporte, km 12+000, Carretera No. 431, “El Colorado, Galindo”, Pedro Escobedo, Querétaro, México, C.P. 76703

\*E-mail: [rantano@cideteq.mx](mailto:rantano@cideteq.mx)

Received: 23 June 2018 / Accepted: 4 October 2018 / Published: 10 May 2019

---

In this study, an evaluation of the corrosion susceptibility of concrete reinforcement steel welded to stainless steel is reported, which is proposed as a potential solution to the repair and rehabilitate structures. An evaluation was conducted over 390 days by measuring the corrosion potential and current density levels by electrochemical impedance spectroscopy applied to a solution that simulated a marine environment. The welded carbon-stainless steel samples were found to be more resistant to corrosion than the carbon steel samples. These results were confirmed by visual inspection, scanning electron microscopy and energy dispersive spectroscopy of the welded zone. These findings support the concept of rehabilitating structures by replacing damaged carbon steel with stainless steel welded to the remaining structures.

---

**Keywords:** Welded zone, Stainless steel-concrete, Marine corrosion, Impedance

## 1. INTRODUCTION

The most common method for reinforcing concrete structures involves the application of carbon steel (CS). Among other functions, concrete protects steel, and together these materials offer very high levels of mechanical resistance [1]. However, carbon steel embedded in concrete is not protected in environments with chloride in which the ions travel throughout the concrete and arrive at the steel surface

[2-3]. Treatment of corrosion phenomena in concrete reinforcement structures is expensive due to continuous service needed after the repair with CS. Generally, the repair and rehabilitation of buildings, bridges, piers and similar structures incurs high economic costs.

Reportedly, annual direct costs of infrastructure corrosion have risen to 2 to 5% of GDP levels in most countries. For example, in USA, yearly corrosion-related expenses are approximately 8 billion USD [4]. Table 1 presents the corrosion-related costs for different countries obtained from the literature [4-7].

**Table 1.** Corrosion related expenses based on the data collected from the literature.

Country	Cost (Billions Of Dollars)	GDP (%)	Year
USA <sup>4</sup>	276	3.1	1999-2001
United Kingdom <sup>5</sup>	0.98		
Peru <sup>6</sup>	1.2	8	2000
Mexico (Veracruz) <sup>7</sup>	0.26		2006

Given the high maintenance costs of concrete infrastructure reinforced with CS, several alternatives have been proposed to mitigate the corrosion phenomena occurring in these concrete structures. Some researchers have proposed various modification of the concrete chemical formulation as reported by Corral, Gutiérrez and Burgos [8–11]. Others such as Al-Zahrani and Vera have studied the use of organic coatings [12–14]. Carvajal, Virides and Herrera have studied the use of inhibitors to prevent reinforcement corrosion [15–17]. On the other hand, Sekar, Calero and Araujo applied a cathodic protection method to reinforcement steel for this purpose [18–20]. Yeomans, Baltazar and Moreno have proposed the use of galvanized steel as an alternative material to extend the lifetime of reinforced concrete structures [21–23]. In another approach, Addari, Luo and Bertolini reported on the use and behavior of stainless steel in an alkaline medium [24-26]. Hunkeler and Jones found that when used as concrete reinforcement, stainless steel lengthens the service times significantly with little or no maintenance required [27-28].

Austenitic (304L and 306L) and duplex (2205 and 2304) stainless steel are most widely recommended for use as concrete reinforcements due to their high corrosion resistance [29]. In particular, austenitic stainless steels are the most widely employed because they are less costly and are resistant to pitting corrosion when exposed to concrete contaminated with chloride ions. Regarding the mechanical properties, stainless steel is twice more ductile than carbon steel. The elongation of stainless steel can exceed 45%, whereas that of carbon steel is roughly 25% [30-31]. Even though stainless steel bars are 5 to 8 times more expensive than carbon steel bars, the use of SS represents an only 10% increase in the overall cost of a project. It has been estimated that its amortization can reduce the initial costs by up to 50% when considering increases in the lifetime that can exceed 120 years in coastal areas [32-33].

The degradation of reinforced concrete structures is typically detected only when the damage levels are significant and repairs are expensive [34-35]. The performance of repaired structures is not

satisfactory. An European special report indicates that 50% of repaired concrete structures have failed [36-37]. Repairs cannot prevent future deterioration and in some cases, they accelerate the rates of damage. Therefore, we seek a means to rehabilitate concrete structures, which in this case refers to “restoration to suitable conditions”. Structural rehabilitation implies improving conditions so that they are superior to initial conditions [34].

Concrete structures can be rehabilitated based on the welding process that offers several advantages such as the opportunity to achieve closer junctions along the borders of the materials with a superior distribution of loads and strains to obtain lighter, resistant, stiff, homogeneous and continuous structures. Nevertheless, this approach also presents some drawbacks (e.g., internal residual stress, risks of fragile breakdown, and fatigue in the sections exposed to dynamic loads) [38].

While several approaches for mitigating the corrosion of concrete structures have been proposed, the replacement of CS with SS has not been widely explored to date. Currently, mechanical connectors are used to join new bars of carbon steel to the remaining carbon steel bars in the concrete structure exposed to a marine environment as depicted in Figure 1. Rehabilitation using carbon steel alone leads to extensive levels of corrosion over a very short period of time, thus incurring excessive costs [39].



**Figure 1.** Example of reparations of reinforced concrete structures based on the use of carbon steel and mechanical connectors.

In this work, the prevention of the corrosion of welded junctions between carbon steel and stainless steel is evaluated. While it may initially be assumed that this type of junction should produce an increase in galvanic corrosion, previous reports have shown that this does not occur [40-41, 42]. Rather, a welded junction should produce more strain spreading while reducing the amount of stainless steel needed for rehabilitation due to its higher mechanical strength. Furthermore, issues such as the buildup of differential aeration cells produced by the presence of mechanical connectors can be avoided when using a welded junction.

## 2. EXPERIMENTAL PROCEDURES

### 2.1. Sample preparation

As shown Table 2, 615 carbon steel and 304L stainless steel rods with chemical compositions (with the diameter and length of 12.7 mm and 200 mm, respectively) were used for the tests. The welded rods were prepared with the same overall dimensions and with the 1:1 area ratio maintained between the carbon steel and the stainless steel zones. For welding, on one end of the rods, a beveled cut with a supplementary angle of  $30^\circ$  was made and a shielded metal arc (SMAW) was applied following the AWS D1.1[43] and NMX H121[44] standards. As a filler material, 309L stainless steel was used as a filler material. To make electrical contact for electrochemical measurements, the end of the copper wire was pressed into the upper predrilled bar end. Then, this junction was sealed with epoxic resin for insulation. The remaining copper wire retained its original plastic insulation. The details of the welded samples (W) are presented in Figure 2. During the tests, the stainless steel is located in the upper part and carbon steel in located in the lower part (Figure 3). The rods were cleaned by abrasion with a brush and were degreased with acetone prior to their embedding in concrete. This latter material was prepared using two different water/cement ratios (w/c) of 0.45 and 0.65, and the dimensions of each cylinder were 100 mm and 220 mm for the diameter and length, respectively. The bar was centered on the cylinder at the distance of 10 mm from the bottom and top (Figure 3). Each sample was fabricated in triplicate. Carbon steel (CS) and stainless steel (SS) samples used as control samples were prepared in a similar manner to those that were used for welding. Concrete cylinders were cured over 28 days according to the C31 ASTM standard [45], and then were partially (more than half submerged) immersed in 3.5% w/w NaCl (Figure 4) to simulate a structure rehabilitated by welding and were exposed to marine environment under static conditions.

**Table 2.** Chemical composition of the steels and filler material electrodes used in this work.

Material	%C	%Cr	%Ni	%Fe
A615	0.24	0.07	0.07	98.3
304L	0.01	18.3	8.07	74.1
309L	0.02	23	13	13

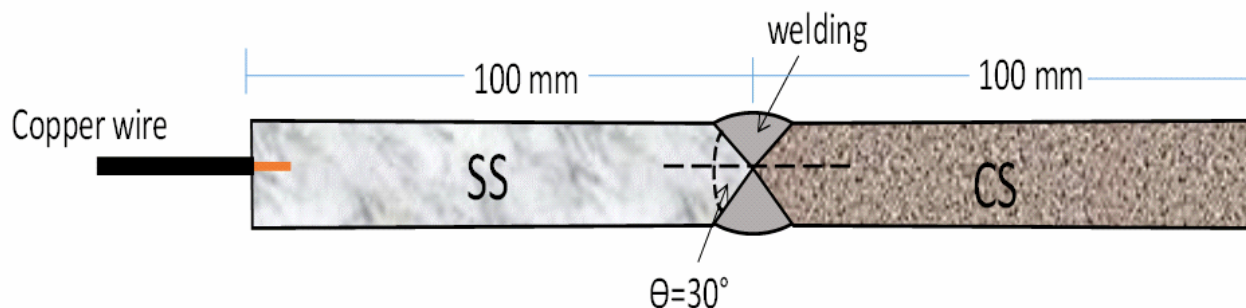


**Figure 2.** Details of the welded rods. CS (carbon steel), SS (stainless steel) and electrical contact (copper wire)

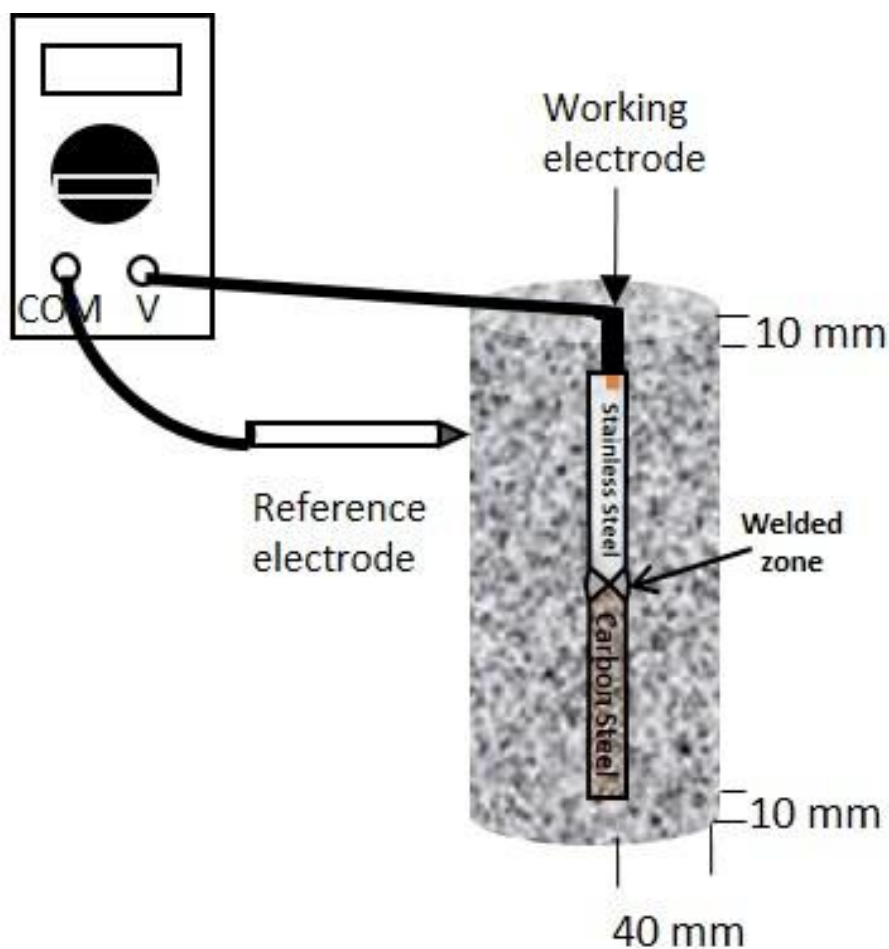


**Figure 3.** Monitoring of the corrosion potential ( $E_{corr}$ ) of the rods embedded in the concrete.

## 2.2. Electrochemical techniques

To monitor the behavior of the phenomena associated with the corrosion of the carbon steel-stainless steel welded junction and the control samples, three electrochemical techniques were employed: corrosion potential ( $E_{corr}$ ) monitoring according to the C876 ASTM standard [46], linear polarization resistance technique (LPR) according to the G59 ASTM standard [47], and electrochemical impedance spectroscopy (EIS) according to the G106 ASTM standard [48]. Corrosion potential monitoring was carried out using a FLUKE 867B multimeter and a Cu/CuSO<sub>4</sub> reference electrode as shown in Figure 3. LPR and EIS measurements were conducted using a Gamry interface 1000 potentiostat. For these tests, metallic rods (W, CS or SS) were connected to the working electrode lead of the potentiostat, and a stainless steel mesh and Ag/AgCl served as the auxiliary and reference electrodes, respectively, as shown in Figure 4. The conditions for the EIS measurements were set as follows: frequencies of 10 kHz to 10 mHz, amplitudes of 2 mV and 8 points per decade. Measurements were performed periodically over 390 days.

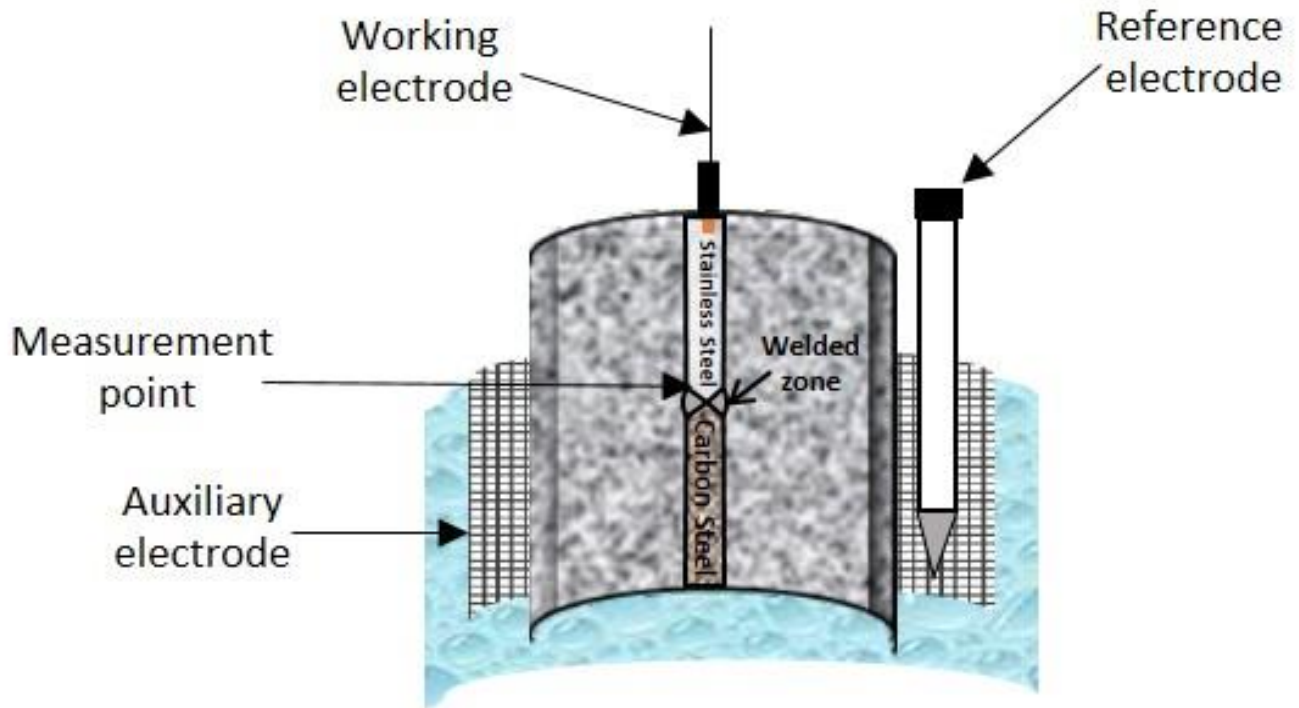


**Figure 4.** Experimental setup used for the linear polarization and EIS measurements. The sample was partially immersed in saline water

### 3. RESULTS AND DISCUSSION

#### 3.1. Corrosion potential

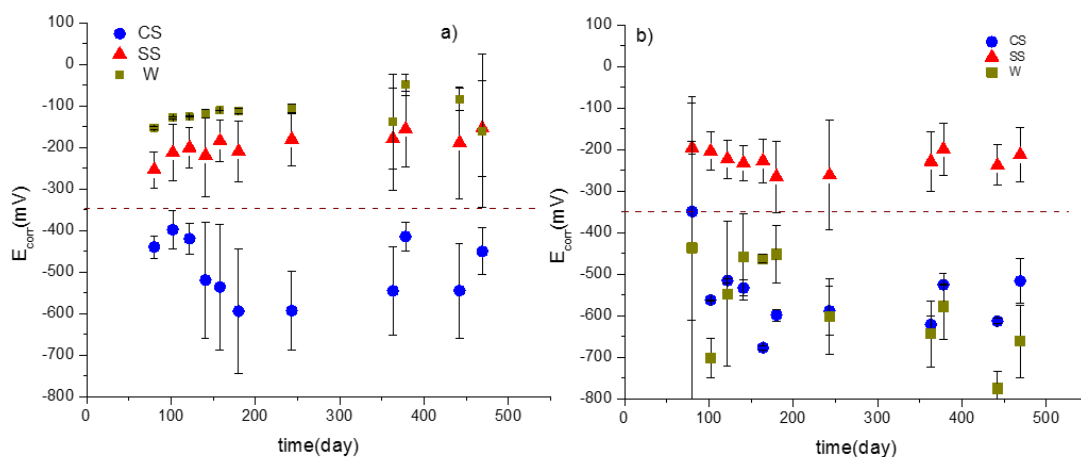


**Figure 5.** Graph of  $E_{corr}$  vs. time for the tested samples partially immersed in saline water a). Water/cement ratio of 0.45. b). Water/cement ratio of 0.65.

Figure 5 shows the  $E_{corr}$  variations with time for the metallic rods of the different samples (W, CS and SS), with the error bars showing one standard deviation. Less significant  $E_{corr}$  variations were found for the 0.45 w/c ratio samples than for those with the w/c ratio of 0.65. For sample W,  $E_{corr}$

ranged from -0.15 to -0.22 V for the first w/c ratio and from -0.1 to -0.5 V for the second w/c ratio. For the CS sample,  $E_{corr}$  values ranged from -0.35 to -0.5 V and from -0.22 to -0.67 for the first and second w/c ratios, respectively. Finally, for the SS sample,  $E_{corr}$  values ranged between -0.1 and -0.2 and between -0.15 and -0.30 for the first and second w/c ratios, respectively.

$E_{corr}$  variations for the W and CS samples were found to be similar to those reported by Qian and Qu [49] (-0.3 V) in their study of CS electrically connected to SS by an external wire. For the SS samples, the obtained range was similar to that reported by Torres [50] (-0.18 V) for the SS embedded in concrete polluted with 2%  $Cl^-$ .

A comparison of the results for the two w/c ratios shows that the CS samples present more negative potentials for the 0.65 w/c ratio than for the 0.45 w/c ratio; therefore, the former is more susceptible to corrosion. It appears that higher water content enhances the inflow of chloride ions, breaking the passive layer generated by the alkaline medium on the surface of the reinforcement, and giving rise to corrosion. The concrete porosity levels depend on the w/c ratio and are favored by the high water content levels in the mix. The remaining fraction of water that is not involved in the hydration reactions evaporates, thus forming porous capillaries in the concrete matrix [51]. Pech [52] found higher ion chloride concentrations in concrete prepared with the 0.7 w/c ratio than in the concrete with the 0.46 w/c ratio due to a higher diffusion of ions in the former, corroborating the Obando's explanation.

It is worth noting that the W and SS samples had  $E_{corr}$  values in the passivation zone according defined by the C876 ASTM standard. By contrast, the  $E_{corr}$  values of the CS samples fall outside of the passivation zone, denoting the occurrence of active corrosion in this case. This behavior was expected because it is well-known that the oxide layer on the surface of carbon steel is less protective than that on stainless steel. Furthermore, the behavior of  $E_{corr}$  for the W samples resembles that of the SS samples more than that of the CS samples. This supports the feasibility of the use of welded stainless steel rather than carbon steel for the rehabilitation of corroded structures.

### 3.2. Corrosion current density levels

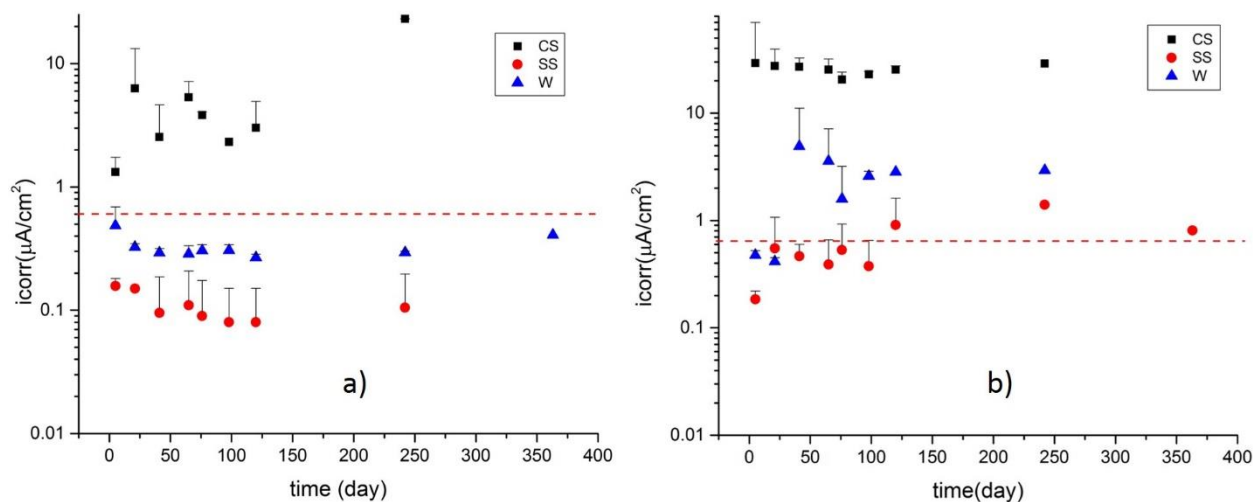


**Figure 6.** Graph of corrosion current density vs. time for the tested samples partially immersed in saline water. a) Water/cement ratio of 0.45. b) Water/cement ratio of 0.65. Potential interval of -20 mV to 20mV. Scan rate of 0.166 mV/s

Figure 6 presents the measured corrosion current density values ( $i_{\text{corr}}$ ) for the different samples. For all of the cases, it was observed that  $i_{\text{corr}}$  is higher for the samples in concrete prepared with the w/c ratio of 0.65, signifying the more extensive corrosion of metallic rods in this type of concrete.

According to the parameters provided by the DURAR handbook regarding the corrosion current density for carbon steel embedded in concrete, the studied W and SS samples present moderate corrosion levels. By contrast, the CS samples present very high corrosion levels for the 0.45 w/c ratio. The samples in concrete with the 0.65 w/c ratio present similar tendencies but with the current density value that is approximately twice as large (especially the CS samples).

The corrosion current density obtained for the CS samples ( $23 \mu\text{A cm}^{-2}$ ) is one order of magnitude larger than that reported by Obando [51] for mortar ( $1.23 \mu\text{A cm}^{-2}$ ). For the SS samples, the obtained value ( $0.12 \mu\text{A cm}^{-2}$ ) was two orders of magnitude higher than that reported by Torres [47] for concrete ( $0.007 \mu\text{A cm}^{-2}$ ). For the W samples, the obtained current density ( $0.31 \mu\text{A cm}^{-2}$ ) was twice that reported by Clemeña [53] for concrete ( $0.15 \mu\text{A cm}^{-2}$ ).

The obtained results confirm that the corrosion rate of carbon steel reinforcement rods is high and that this is due to the presence of chloride ions. These ions have two effects on the corrosion mechanisms. The ions increase the ionic conductivity of the electrolytes, enhancing ionic transport and provoking the local disruption of the passive layer.

### 3.3. Electrochemical impedance spectroscopy

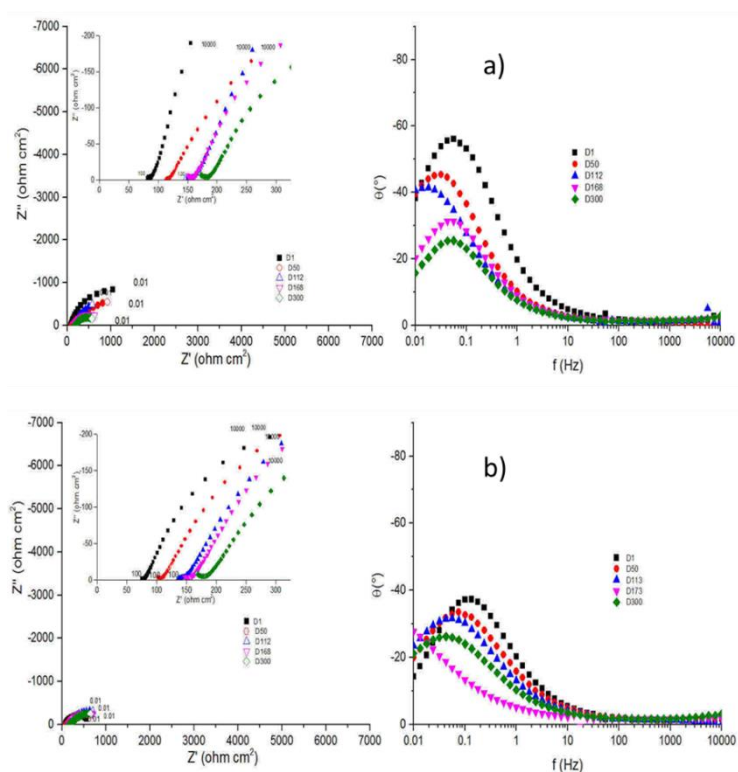


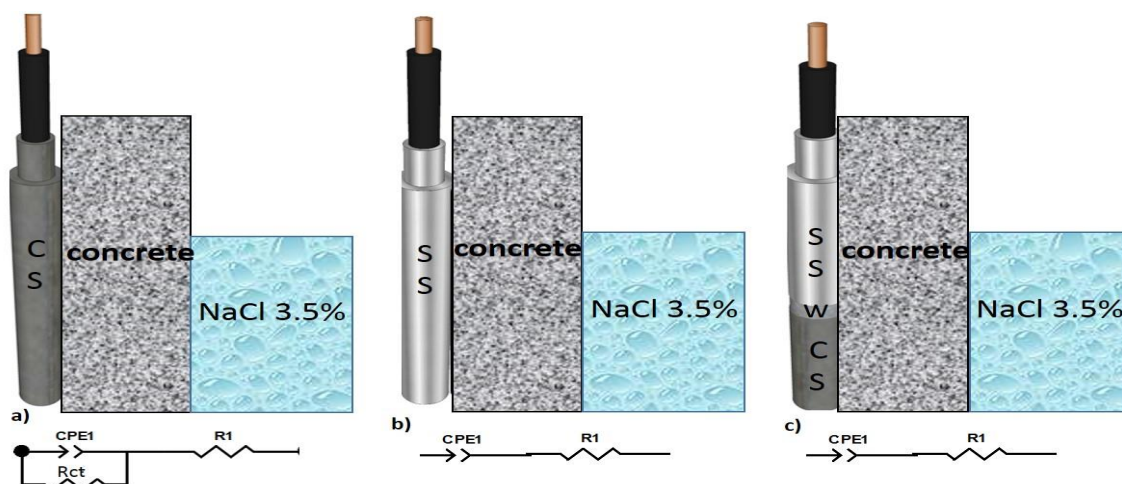
**Figure 7.** Nyquist and Bode diagrams of carbon steel embedded in concrete with a) water/cement ratio of 0.45 and b) water/cement ratio of 0.65, both partially immersed in saline water. The parameters of the measurements were as follows: frequencies of 10 kHz to 10 mHz and amplitudes of 2 mV and 8 points per decade.

Figures 7, 9 and 10 show the Nyquist and Bode diagrams for the samples prepared with both w/c ratios. We start here by discussing the results found for the nonwelded materials, i.e., the CS and SS samples, in order to validate these results by comparison to the corresponding results in the literature, and we then establish them as a reference for examining and understanding the results found for the welded samples.

### 3.4. Carbon steel samples

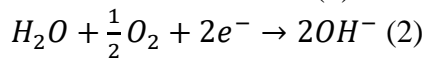
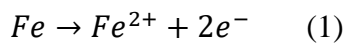
Figure 7 shows the Nyquist and Bode diagrams for the CS samples. In these diagrams, a semicircle with a diameter that decreases with time is observed. This diameter defines the charge transfer resistance ( $R_{ct}$ ) that represents the opposition of the interface to the passage of electrical currents. It was found that  $R_{ct}$  is three times higher for the samples with the 0.45 w/c ratio than for those with the 0.65 ratio, denoting higher levels of corrosion resistance for the CS samples with the first ratio.

The CS samples present resistant behavior in the low frequency range, implying the presence of an active interface. The Bode-phase diagram shows angles of less (in absolute terms) than  $-60^\circ$ . It is known that angles tending toward  $0^\circ$  are indicative of resistive behavior whereas the angles tending toward  $-90^\circ$  are indicative of capacitive behavior [54]. Here, we find both types of contributions. Figure 8a presents a schematic of the equivalent circuit proposed for modeling the CS samples' spectra. This circuit is composed of a constant phase element (CPE) that represents the nonideal capacitance of the double layer that is connected in parallel to  $R_{ct}$  and to  $R_1$  that represents the electrolyte resistance. This latter term considers the resistance of concrete and saline dissolution. Since there is no evidence of the specific trace given by the diffusion in the spectra, it is assumed that the main contribution to impedance is a result of charge transfer, signifying the activated control of the overall process rate. The corrosion potential values recorded during these tests were less than  $-350$  mV due to the changes in the thermodynamics of the CS sample surface where the instability of the passive layer induced by chloride ions is prevalent.



**Figure 8.** Schematic of the equivalent circuit elements representing the physical systems: a). carbon steel; b). stainless steel; c). carbon steel welded to stainless steel.

Similar spectra and equivalent circuits were reported by Corral [8] for a study of carbon steel in concrete with the 0.47 w/c ratio. Our spectra agree with Nyquist diagrams reported by Perez [55] for concrete reinforced with carbon steel. He proposed an equivalent circuit that adds a diffusion component, but as noted above, there is no evidence of this contribution in the corresponding diagrams. Bensabra and Azzouz [56] studied carbon steel exposed for a short time to a pore solution with added chloride ions (3%) and their results agree with our results. Pech and Castro [52] studied concrete samples reinforced with carbon steel and exposed to natural weathering in the marine atmosphere, and presented Nyquist diagrams with the 45° linear tendency in the low frequency region typical of diffusive contributions. In this case, the Warburg element in the equivalent circuit is justified. With regard to capacitive contributions, our results agree with those reported by Andrade [57] in a study of carbon steel in concrete with added 2% CaCl<sub>2</sub>, with those of Rendon [58] in a study of carbon steel embedded in the 0.48 w/c ratio concrete exposed to sea water, and with those of Sagües and Cui [59] in a study of carbon steel in a pore solution. Since alkaline medium was in this work and in the cited studies, the expected anodic and cathodic reactions are as follows:



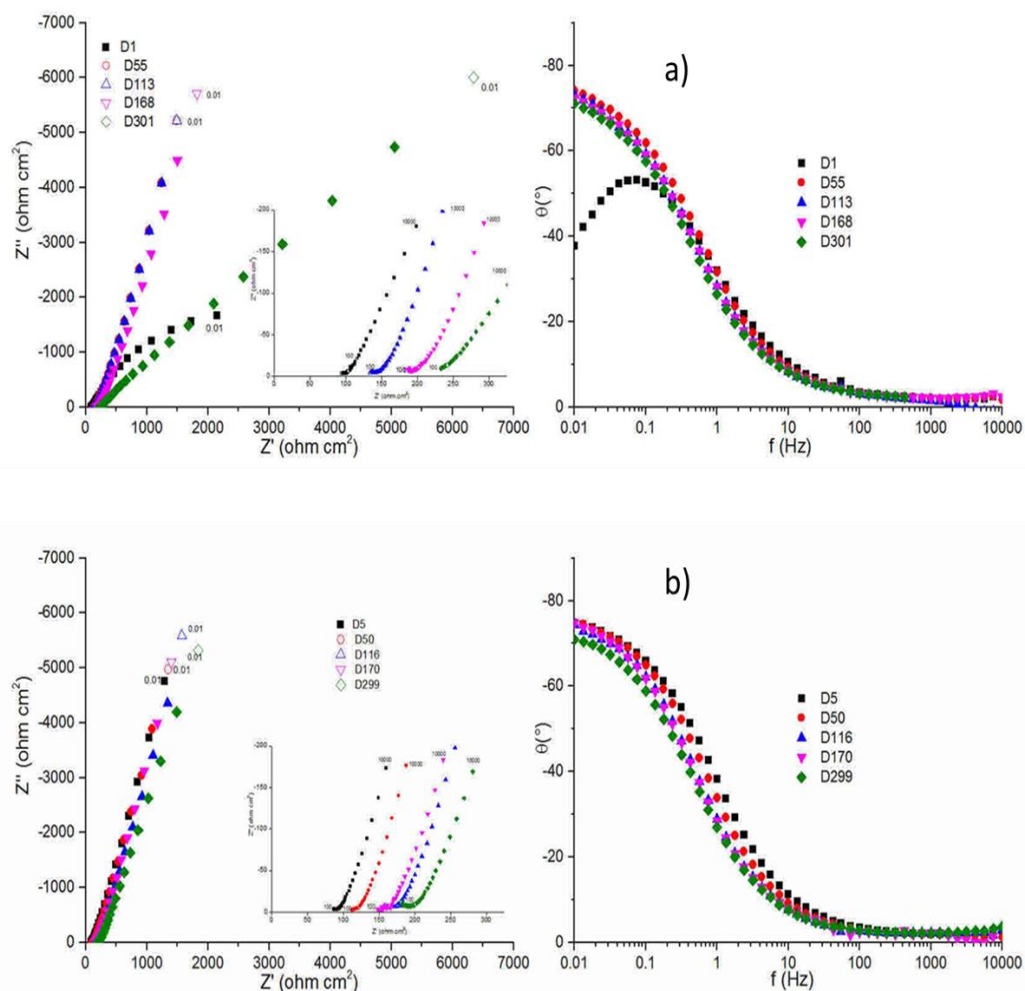
### 3.5. Stainless steel samples

Figure 9 shows the Nyquist and Bode diagrams for the SS samples. The Nyquist diagram shows the start of a semicircle with an extrapolated  $R_{tc} \approx 5400$  for the first day, showing that corrosion is occurring even though it is incipient. However, the spectra for the following days show the complete predominance of capacitive behavior. This is corroborated in the Bode-phase diagram, where the angle approaches -75° in the low frequency range. This is attributed to the well-recognized passivation phenomena occurring along the surfaces of the stainless steel.

The proposed equivalent circuit shown in Figure 8b is designed to model this capacitive behavior. The circuit includes a CPE element to represent the nonideal capacitance of the steel-concrete interface coupled in series to R1 that represents the conductive properties of concrete and saline solution. According to Andrade, in this type of system with stainless steel, a layer of corrosion products is generated along the stainless steel surface. These products are metallic oxides that passivate the metallic surface and hinder the charge transfer. The  $E_{corr}$  values monitored during these tests are more anodic than -350 mV, showing that according to the ASTM C876 standards, this stainless steel is in the passive zone, in complete agreement with the EIS results.

Blanco [60] have studied 304 stainless steel samples in pore solution with added 1% chloride and presented a Nyquist diagram for which the spectra are similar to those found in this work for the initial day. However, over the following days, the spectra observed in our study shifted to capacitive behavior. This behavior has been reported by Sagües [59] and Li [61] in their study of 316 stainless steel samples in pore solution and of 304 stainless steel samples in the pore solution with added 3.5% chlorides.

The results discussed above validate the results found for the CS and SS samples under the studied conditions and support the discussion of the welded samples presented below.



**Figure 9.** Nyquist and Bode diagram of stainless steel embedded in concrete with a) water/cement ratio of 0.45 and b) water/cement ratio of 0.65, both partially immersed in saline water. The parameters used for the measurements were as follows: frequencies of 10 kHz to 10 mHz and amplitudes of 2 mV and 8 points per decade.

### 3.5. Welded samples

A further inspection of the spectra corresponding to each sample type allows us to infer that resistance to the charge transfer occurs in the following order  $SS > W > CS$ . This was expected, because the welded samples include both materials and the welded zone should share their properties. The equivalent circuit for modeling these spectra (Figure 8c) is the same as that proposed for the SS samples due to the similarity of their spectra. The associated capacitance for the W samples (Figure 10) is also similar to that of the SS samples, denoting the enhanced corrosion resistance of the W samples relative to the CS samples. These results and the capacitive impedance suggest that the W samples were passivated by an insulating film similar to the SS samples but that the former were less protective than

the latter [62]. The capacitance values for the W and SS samples are lower than those obtained for the CS samples due to the less compact insulating film on the latter. Cathodic and anodic reactions observed for the W samples are assumed to be the same as those found for the CS samples but are hindered to a certain degree by the presence of the insulating film. This film acts as an ideally polarizable electrode (mainly the capacitive contribution) where the charge transfer resistance is so large that corrosion reactions can be considered negligible. It is worth mentioning that because the corrosion process observed from the W samples was small, galvanic corrosion levels were also low for these samples.

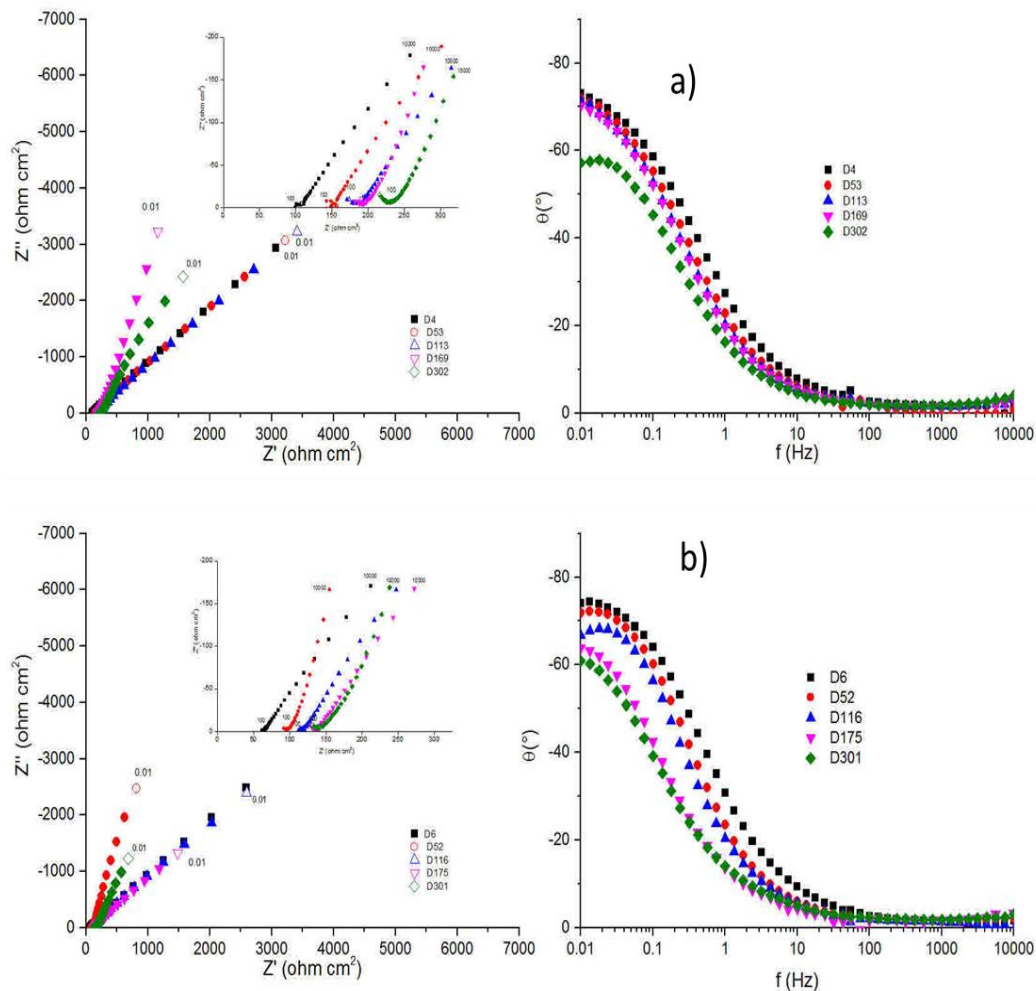


**Figure 10.** Nyquist and Bode diagrams of stainless steel welded to carbon steel embedded in concrete with a) water/cement ratio of 0.45 and b) water/cement ratio of 0.65, both partially immersed in saline water. The parameters used for the measurements were as follows: frequencies of 10 kHz to 10 mHz and amplitudes of 2 mV and 8 points per decade.

According to Le Bozec [63], along the passivated surfaces of stainless steel, oxide films have a bilayer structure with iron or chromium oxides in the inner layer and chromium hydroxide in the external layer. They remark that both chromium oxide and hydroxide inhibit oxygen reduction reactions because they limit the diffusion of oxygen to the substrate. Kappler and Goellner [64] confirmed that the kinetics of oxygen reduction on surfaces with more stable passive films are slower than those of surfaces covered with iron oxide, showing that Fe(II) sites act as catalysts to reduce oxygen levels. Our findings agree

with these results and are reinforced by the images of the samples taken after the end of the test. The surfaces of the rods of the SS samples were entirely free of corrosion products for both w/c ratios. For the W samples, the samples prepared with the 0.45 w/c ratio had surfaces free of corrosion products whereas those prepared with the 0.65 ratio had corrosion products along the side corresponding to carbon steel. This highlights the importance of the w/c ratio for the definition of the susceptibility of the systems to be corroded. On the other hand, the CS samples with the 0.65 w/c ratio presented larger accumulations of corrosion products.

The welded rods embedded in concrete and exposed to saline medium can spur oxygen reduction over three steps (including adsorption-desorption), implying the presence of oxygen-containing species such as  $O_2$ ,  $OH^-$ ,  $O_2^-$ ,  $HO^{2-}$  and  $H_2O_2$  [65]. According to Ge [65], oxygen reduction is limited along the stainless steel surfaces. This is related to the low adsorption energy levels of anions in alkaline pH (e.g., chloride ions when they arrive at the surface).

The observed capacitive behavior that implies the passivity of the welded junction in the W samples can be explained by the theory proposed by Novoa [66] for the surface character of stainless steel. He proposed that the presence of chromium in the internal planes of the film obtained with exposure in alkaline medium protects against corrosion because it forms shields or islands of chromium (III) oxide that protect the substrate. It is noted that chromium oxide is more stable than iron oxide because its Gibbs free energy is more negative [67]. Chromium can be oxidized by water while iron requires oxygen to be oxidized [68]. Furthermore,  $Cr_2O_3$  is a dielectric whereas iron oxides are semiconductors unlike magnetite ( $Fe_3O_4$ ) which is a good electrical conductor. The partial electrical insulation of stainless steel by  $Cr_2O_3$  leads to a weaker transfer of electrons onto the stainless steel than onto the fully conductive carbon steel [67, 69]. As a result, stainless steel is a poor cathode of the overall corrosion process, thus minimizing the problematic corrosion occurring in the adjacent carbon steel for welded samples. This also occurs in its passive state after rehabilitation.

Over time, the W and SS samples exhibited higher levels of corrosion resistance than the CS samples. This is also attributed to the passive film on the surface that is always prevalent because the alkaline medium provides  $OH^-$  ions that undergo adsorption on the passive film [70-71]. This enhances its reconstruction and hinders the arrival of  $Cl^-$  ions to the passive film and thus to the iron substrate [72].

### 3.6. Autopsy and SEM results

After 390 days of exposure to chloride ions and concrete, one bar of each sample type was removed, and an autopsy was conducted to confirm the results of the electrochemical tests. Each sample was photographed and scanning electron microscopy (SEM, HITACHI 3700N) images were obtained to document any corrosion products. Figures 11 and 12 present the obtained macroscopic and SEM images.

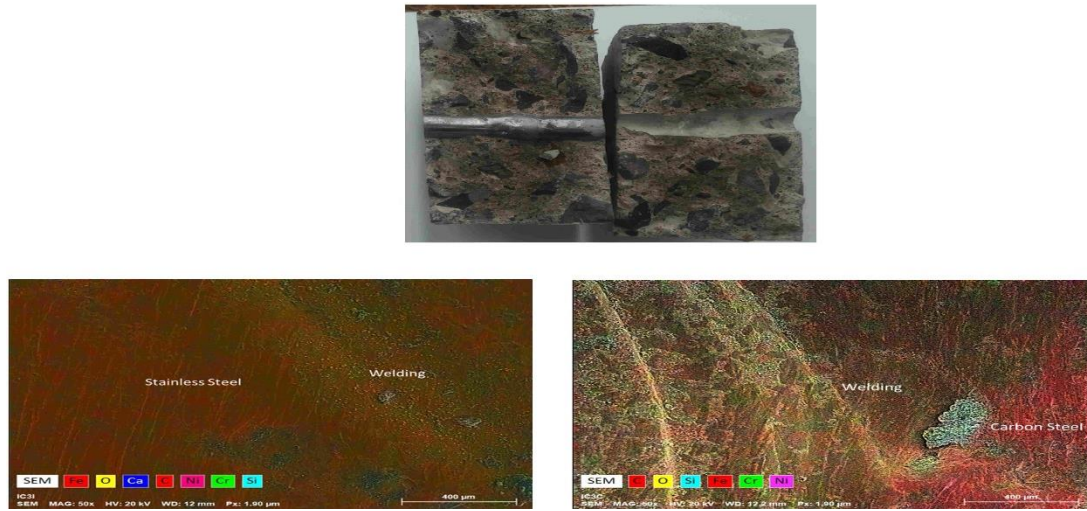


**Figure 11.** Image taken after testing and SEM micrographs of carbon steel welded to stainless steel and embedded in concrete with the 0.45 water/cement ratio and partially immersed in saline water.

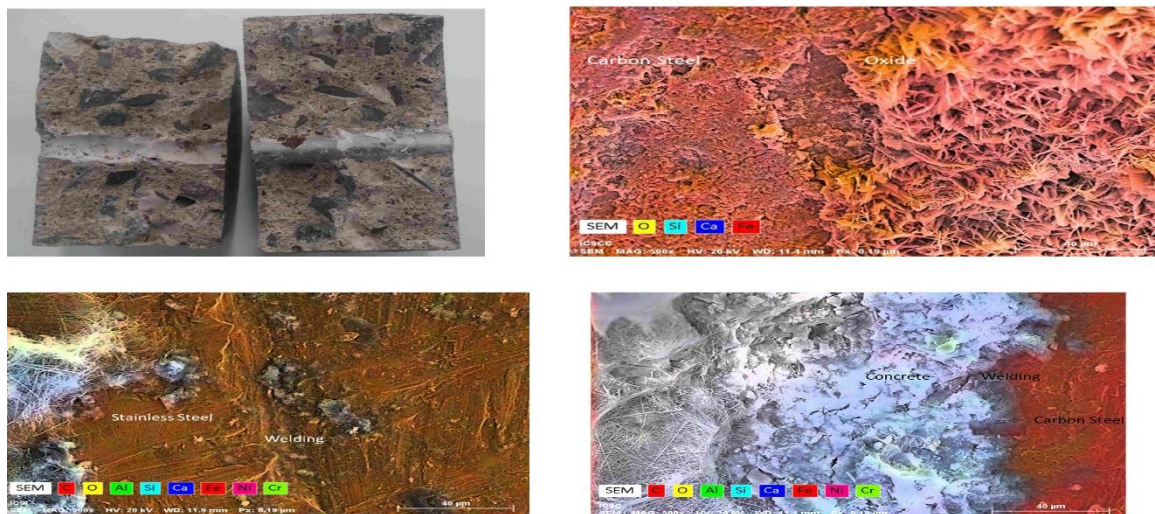


**Figure 12.** Image taken after testing and SEM micrographs of carbon steel welded to stainless steel and embedded in concrete with the 0.65 water/cement ratio and partially immersed in saline water.

Figures 11 and 12 confirm the results obtained by electrochemical techniques applied to the samples embedded in concrete samples with 0.45 and 0.65 w/c ratios. It is worth noting that the samples embedded in concrete with the 0.45 w/c ratio for which the micrographs are presented in Figures 11 did not develop corrosion products. This is mainly attributed to the protective properties of concrete prepared with this ratio. Figure 12 indicates that incipient corrosion products were present in the carbon steel zone of the welded sample, while negligible corrosion products were observed in the welded zone, and as expected, a clean surface was observed on the stainless steel side. By contrast, abundant corrosion products were found in the CS control sample (not shown).

On the other hand, similarities in the behaviors of the W and SS samples confirm that galvanic corrosion produced by the junction between carbon steel and stainless steel was negligible in this case.

This is in agreement with the results of the works of Le Bozec [63] and Keppler [64] who concluded that this behavior is due to the deficient supply of stainless steel electrons, which in turn limits oxygen reduction as discussed above.

#### 4. CONCLUSIONS

❖ It was found that the samples for which carbon steel is welded to stainless steel are less susceptible to corrosion than carbon steel alone under simulated marine dissolution conditions as found by Ecorr monitoring, linear polarization and EIS techniques.

❖ Our EIS results show that welded samples exhibit more capacitive behaviors and thus develop a passivated surface and therefore exhibit less corrosion.

❖ An autopsy conducted on the samples after the test confirmed the absence of corrosion products in the welded junction. It was concluded that galvanic corrosion levels are negligible under the studied conditions.

❖ Higher levels of corrosion resistance were found for concrete-embedded samples prepared with the 0.45 w/c ratio than for those prepared with the 0.65 w/c ratio; therefore, this is a critical parameter that must be considered for improving the corrosion resistance. For each w/c ratio, the corrosion resistance values of the tested samples were in the following order: stainless steel > welded SS-CS > carbon steel.

#### ACKNOWLEDGEMENT

The first author is grateful for the grant awarded to Consejo Nacional de Centro y Tecnología (CONACYT). The authors are grateful for the facilities granted to the Centro de Investigación y Desarrollo Tecnológico en Electroquímica (CIDETEQ) as well as Instituto Mexicano del Transporte (IMT). The authors thank Dr. Fabricio Espejel and Eng. Maura Arroyo for their support with SEM and EDS measurements.

#### References

1. U. Angst, M. Geker, A. Michel, C. Gehlen, H. Wong, O. Burkan, B. Elsener, C. Hansson, R. Francois, K. Hornbostel, R. Polder, M. Alonso, M. Sanchez, M. Correira, M. Criado, A. Sagües and N. Buenfeld, *Mater. Struct.*, 50 (2017) 142.
2. H. Böhni, *Corrosion in reinforced structures*, CRC 2005.
3. P. Terradillos, C. Llorca and E. Gómez, *Corrosión de armaduras en estructuras de hormigón armado*, Club Universitario 2008.
4. H. Koch, P. Brongers, G. Thompson, P. Virmani and H. Payer, *NACE Int.*, (2002) 3.
5. O. Troconis, A. Romero, C. Andrade, P. Helene and I. Díaz, *Manual de inspección, evaluación y diagnóstico de corrosión en estructuras de hormigón armado*, CYTED 2000.
6. J.L. Ramírez, D. Pereyra, N. García, L. Valencia and V. Juárez, *Atmosfera*, 25 (2012) 397.
7. J.L. Ramírez, D. Pereyra, N. García, L. Valencia and V. Juárez, *Revista de Divulgación Científica y Tecnológica de la Universidad Veracruzana*, 24 (2011) 1.
8. R. Corral, S. Arredondo, J. Almaral and J. Gómez, *Revista Ingeniería de Construcción RIC*, 28 (2013) 21.

9. M. Burgos, E. Angulo and R. Mejía de Gutiérrez, *Revista Ingeniería de Construcción RIC*, 28 (2012) 61.
10. O.J. Gutiérrez, Y. Pineda and E. Vera, *Rev. LatinAm. Metal. Mat.*, 32 (2015) 1.
11. O. Gutiérrez, Y. Pineda and E. Vera, *Rev. Metal.*, 51 (2015) 58.
12. M. Al-Zahrani, U. Al-Dulaijan, M. Ibrahim, H. Saricimen and M. Sharif, *Cem. Concr. Compos.*, 24 (2002) 127.
13. R. Vera, J. Apablaza, A.M. Carvajal, *Rev. la Construcción*, 4 (2005) 13.
14. L. Shi and J. Liu, *Procedia Engineering*, 27 (2012) 291.
15. A. Carvajal, *Rev. la Construcción*, 4 (2005) 25.
16. I. Vyrides, E. Rakanta, T. Zafeiropoulou, and G. Batis, *Open J. Civ. Eng.*, 3 (2013) 1.
17. H. Herrera-Hernández, M. Franco-Tronco, J. Miranda-Hernández, E. Hernández-Sanchez, A. Espinoza-Vázquez and G. Fajardo, *Av. en Ciencias e Ing.*, 6 (2015) 9.
18. S. Sekar, V. Saraswathy and T. Parthiban, *Int. J. Electrochem. Sci.*, 2 (2007) 872.
19. A. Araujo, Z. Panozian and Z. Laurengo, *Ibracon Struct. Mater. J.*, 6 (2013) 178.
20. C. Calero, C. Llorca and P.G. Terradillos, *J. Electroanal. Chem.*, 793 (2016) 8.
21. S. Yeomans, Galvanized steel reinforcement of concrete, Elsevier 2004.
22. M. Baltazar-Zamora, E. Maldonado-Bandala, M. Loya, G. Santiago-Herrera, F. Olguín, A. Ortíz-Cedano, C. Barrios, R. Niñez, P. Zambrano, C. Gaona and F. Almeraya, *Int. J. Electrochem. Sci.*, 7 (2012) 2997.
23. I. Moreno, S. Ixtepan and C. Sarabia, *Ingeniería*, 9 (2005) 17.
24. D. Addari, B. Elsener and A. Rossi, *Electrochim. Acta*, 53 (2008) 8078.
25. H. Luo, F. Dong, G. Li and K. Xiao, *Electrochim. Acta*, 64 (2012) 211.
26. L. Bertolini, M. Gastaldi, M. Pedferri and P. Pedferri, *Br. Corros. J.*, 31 (1996) 218.
27. F. Hunkeler, TFB CH-5103 Wildeg, (2001) 1.
28. CD Jones, 3CR12CROMWELD Stainless steel, 01 (2001) 1.
29. A. Goyal, H. Sadeghi, E. Ganjian and P. Claisse, *Arab J Sci Eng.*, (2018) 1.
30. J. F. McGurn, International Conference of Corrosion and Rehabilitation of Reinforced Concrete Structures, Orlando, 1998.
31. I. Tylek and K. Kuchta, *Technical Trans. Civ. Eng.*, 12 (2014) 59.
32. A. Cobo, D. Bastidas, M. Gonzalez and E. Medina, *Mater. Construcción*, 61 (2011) 613.
33. D. Cramer, S. Covino, S. Bullard, G. Holcomb, J. Russell, F. Nelson, H. Laylor and S. Soltesz, *Cem. Concr. Compos.*, 24 (2002) 101.
34. O. Hernández-Castañeda and C.J. Mendoza-Escobedo, *Ing. Investig. y Tecnol.*, VII (2006) 58.
35. S. Suryawanshi, *Indian Concr. J.*, (2012) 37.
36. J.P. Broomfield, Corrosion of steel in concrete, CRC 2006.
37. Z. Taffesea, and E. Sistonen, *Procedia Eng.*, 57 (2013) 1138.
38. A. Picazo, I Jornada Nacional de Investigación en Edificación, Madrid, 2007.
39. A. Castañeda and M. Rodríguez, *Revista CENIC*, 45 (2014) 52.
40. C. Abreu, Cristobal, M.F. Montemor, X.R. Nova, G. Pena and M. Perez, *Electrochim. Acta*, 47 (2002) 2271.
41. F. Xingguo, L. Jing, H. Cen, L. Zuocheng, J. Yukun and C. Xu, *Int J. Electrochem Sci*, 11 (2016) 5226.
42. J. Lopes, M. Stecanella, A. Araujo, J. Serra and Z. Pannossian, NACE Corrosion Conference & Expo, Arizona 2018.
43. AWS D1, Structural Welding Code- Reinforcing Steel 2011.
44. NMX-H-121, Procedimiento de soldadura estructural para acero de refuerzo 1988.
45. ASTM C31, Cast and laboratory cure two sets of two standard cylinder specimens for each composite sample 2003.
46. ASTM C 876 Standard Test Method for Half-Cell Potentials of Uncoated Reinforcing Steel in Concrete 2009.

47. ASTM G59 Standard Test Method for Conducting Potentiodynamic Polarization Resistance Measurements.
48. ASTM G106 Standard Practice for Verification of algorithm and Equipment for Electrochemical Impedance Measurements 2004.
49. S. Qian and D. Qu, 14<sup>th</sup> Asian Pacific corrosion control conference, China 2006.
50. A. Torres, J. Pérez, A. Ramírez, M. Martínez, Secretaria de Comunicaciones y Transporte, Instituto Mexicano del Transporte, 287 (2006) 59.
51. M. Kumar, N. P. Singh, N. B. Singh *Indian J Chem Technol*, 16 (2009) 499.
52. M. Peach-Canul and P. Castro, *Cem. Concr. Res.*, 32 (2002) 491.
53. G. Clemeña and P. Virmani, VTRC 03-R6, 2002.
54. V. Lvovich, Impedance Spectroscopy Application to electrochemical and dielectric phenomena, WILEY 2012.
55. T. Pérez, Aplicación de la técnica Espectroscopía de Impedancia Electroquímica (EIS) en el estudio de la corrosión del acero de refuerzo embebido en concreto, *Programa de corrosión del Golfo de México*, 2002.
56. H. Bensabra and N. Azzouz, *Metall. Mater. Trans. A*, 44A (2013) 5703.
57. C. Andrade, M. Keddad, X. Novoa, M. Perez, C. Rangel and H. Takenouti, *Electrochim. Acta*, 46 (2001) 3905.
58. M. Rendón, M. Martínez, J. Perez-Quiroz, B. Valdez, E. Salas, A. Juarez and M. Schorr, *Anti-Corrosion Methods Mat.*, 62 (2015) 69.
59. F. Cui, and A. Sagüés, *CORROSION*, 4 (2008) 1.
60. G. Blanco, A. Bautista and H. Takenouti, *Cem. Concr. Compos.*, 28 (2006) 212.
61. L. Li, F. Dong, K. Xiao, Z. Yao, and G. Li, *Constr. Build. Mater.*, 68 (2014) 709.
62. V. Millano, M. Sanchez, O. Troconis, D. Linares and N. Romero, *Rev. Tec. Ing. Univ. Zulia*, 29 (2006) 291.
63. Le Bozec, C. Compere, M. L'Her, M. Laouenan, D. Costa and P. Marcus, *Corros. Sci.*, 43 (2001) 765.
64. K. Helmuth, J. Goellner, *Corros. Sci.*, 51 (2009) 144.
65. X. Ge, A. Sumboja, D. Wu, T. An, B. Li, F. Goh, T. Hor, Y. Zong, and Z. Liu, *ACS Catal.*, 5 (2015) 4643.
66. M. Bastidas and E. Medina, Armaduras de acero inoxidable, CEDINOX201 2013.
67. M. Schutze, Protective oxide scales and their breakdown, John Wiley & Sons 1997.
68. A. Bard, Encyclopedia of electrochemistry of the elements, Marcel Dekker 1986.
69. J. Jiang, D. Wang, H. Chu, H. Ma, Y. Liu, Y. Liu, Y. Gao, J. Shi, and W. Sun, *Materials*, 10 (2017) 412.
70. P. Marcus, Corrosion mechanisms in theory and practice, CRC Press 2012.
71. V. Maurice and P. Marcus, *Electrochim. Acta*, 84 (2012) 129.
72. P. Marcus, *Electrochim. Acta*, 43 (1998) 109.